Natural Resources Research, Vol. 25, No. 4, December 2016 (© 2016)
DOI: 10.1007/s11053-016-9290-7

An AHP–TOPSIS Predictive Model for District-Scale Mapping of Porphyry Cu–Au Potential: A Case Study from Salafchegan Area (Central Iran)

Hooshang H. Asadi,[1,2,6] Atefeh Sansoleimani,[3] Moslem Fatehi,[1] and Emmanuel John M. Carranza[4,5]

Received 17 September 2015; accepted 4 January 2016
Published online: 2 March 2016

The Salafchegan area in central Iran is a greenfield region of high porphyry Cu–Au potential, for which a sound prospectivity model is required to guide mineral exploration. Satellite imagery, geological geochemical, geophysical, and mineral occurrence datasets of the area were used to run an innovative integration model for porphyry Cu–Au exploration. Five favorable multi-class evidence maps, representing diagnostic porphyry Cu–Au recognition criteria (intermediate igneous intrusive and sub-volcanic host rocks, structural controls, hydrothermal alterations, stream sediment Cu anomalies, magnetic signatures), were combined using analytic hierarchy process and technique for order preference by similarity to ideal solution to calculate a final map of porphyry Cu–Au potential in the Salafchegan area.

KEY WORDS: Porphyry Cu–Au, AHP–TOPSIS, Data integration, Central of Iran.

INTRODUCTION

Different data integration algorithms, which have been used for mineral potential mapping in recent years, are categorized as either data driven or knowledge driven (Bonham-Carter 1994; Pan and Harris 2000; Carranza 2009, 2011; Abedi et al. 2013). Examples of data-driven techniques are artificial neural networks (Porwal et al. 2003a; Abedi and Nouruzi 2012), weights-of-evidence (Bonham-Carter et al. 1989; Asadi and Hale 2001; Ford et al. 2015), support vector machine (Zuo and Carranza 2011; Abedi et al. 2012b; Geranian et al. 2015), and random forests (Carranza and Laborte 2015a, b, c; McKay and Harris 2015). In these and other data-driven techniques, known mineral deposits in a region of interest are used as 'training points' to establish spatial relationships with particular geological, geochemical, and geophysical features (Carranza et al. 2008; Abedi et al. 2013). These methods are appropriate for well-explored regions and the trained model is used for extracting features that are similar to those associated with known mineral deposits in a study area. Knowledge-driven techniques are suitable for greenfields or less-explored regions (Carranza 2011). In these techniques, the prepared predictor maps are combined based on

[1]Department of Mining Engineering, Isfahan University of Technology, 8415683111, Isfahan, Iran.
[2]Centre for Exploration Targeting, Australian Research Council Centre of Excellence for Core to Crust Fluid Systems, School of Earth and Environment, The University of Western Australia, Crawley, WA 6009, Australia.
[3]School of Earth Sciences, The University of Queensland, Brisbane, QLD 4072, Australia.
[4]Economic Geology Research Centre, College of Science, Technology and Engineering, James Cook University, Townsville, QLD, Australia.
[5]Institute of Geosciences, State University of Campinas, Campinas, São Paulo, Brazil.
[6]To whom correspondence should be addressed; e-mails: hooshang.asadiharoni@uwa.edu.au, hooshang@cc.iut.ac.ir

the expert opinion. The most commonly used methods of this category are index overlay (Bonham-Carter et al. 1989; Carranza et al. 1999; Yousefi and Carranza 2015) and fuzzy logic (An et al. 1991; Porwal et al. 2003b; Abedi et al. 2012c). Porwal et al. (2004) and Asadi et al. (2015) used a hybrid fuzzy-neural network data integration modeling. In this type of modeling, expert knowledge is used for weighing the spatial proxies, and the weights are fine-tuned using a neural network which is trained by known mineral occurrences.

Mineral potential mapping is a multi-criteria decision making (MCDM) activity (Abedi et al. 2012a, d, 2013). Various MCDM algorithms have been used as a tool for mineral potential mapping by Pazand et al. (2011, 2012) and Abedi et al. (2012a). They proposed ELECTRE (Abedi et al. 2012d) and PROMETHEE (Abedi et al. 2012e) algorithms as knowledge-driven techniques for mineral potential mapping and used these methods for finding the best location for extra drilling in a copper deposit. Pazand et al. (2012) proposed the TOPSIS method as a tool for preparing prospectivity maps for porphyry copper exploration. The analytic hierarchy process (AHP) is another MCDM technique, which needs a pairwise comparison matrix for determination of weights of exploration criteria, that is used in mineral potential mapping (Hosseinali and Alesheikh 2008; Pazand et al. 2011; Abedi et al. 2013). Pazand and Hezarkhani (2015) proposed a combined AHP–TOPSIS method to map porphyry Cu potential in Siahrud area, NW Iran.

In this paper, the integrated AHP–TOPSIS algorithm, initially proposed by Pazand and Hezarkhani (2015), was used to map high-potential zones in an area in central Iran with very few known mineral deposit occurrences. The proposed algorithm consists of two main steps. In the first step, the criteria weight vector is obtained from the AHP. In the second step, the TOPSIS algorithm is used for integration of different data sets. TOPSIS is based on the distance of attributes (pixels are considered as attributes) to positive (best alternative) and negative (the worst alternative) ideal solution. The ideal solutions are determined by the user or from existing data. Simplicity and no need of prior knowledge by decision maker are the most important advantages of this method in comparison to other MCDM algorithms such as ELECTRE (Abedi et al. 2012d), PROMETHEE (Abedi et al. 2012e), and the well-known fuzzy logic method (Porwal et al. 2003a, b). The only requirement in the TOPSIS method is the criteria weight vector as other knowledge-driven algorithms that are determined in the first step by AHP method.

The proposed algorithm is demonstrated here for mapping favorable areas of porphyry Cu–Au mineralizations in the northern part of the 1:100,000 scale Salafchegan geological map sheet, which contains very few known porphyry Cu–Au occurrences. The Salafchegan area is a sparsely vegetated and mountainous region, located in the central part of Urumieh–Dokhtar volcanic arc (UDMA), the main porphyry copper belt of Iran (Fig. 1). Dalli, with a total inferred resource of 20 million tons at 0.5 % Cu and 0.65 g/t Au, is the largest porphyry Cu–Au deposit in the central UDMA. Spectral remote-sensing and catchment basin analysis of stream sediment geochemical data were employed, respectively, to map hydrothermal alterations and geochemical signatures that could be associated with this type of mineralization. Magnetic data were interpreted to map intrusive rocks and structures associated with porphyry Cu–Au mineralization. Then, an integrated AHP–TOPSIS model was used as an innovative integration modeling approach to integrate geological, spectral, magnetic, and geochemical datasets. This integration model takes advantages of the MCDM, and the results were used to construct a predictive model to locate high-potential areas of porphyry Cu–Au mineralizations for district-scale exploration in the study area.

BACKGROUND THEORY OF PROPOSED AHP–TOPSIS ALGORITHM

In the AHP–TOPSIS data integration approach, the weight vector of criteria for input exploration data is calculated primarily using the AHP method. Then, if an acceptable consistency ratio is obtained, the alternatives are ranked using the TOPSIS method. The background theory of AHP and TOPSIS methods is explained in the following paragraphs.

AHP

The AHP was proposed by Saaty (1977, 1980) to model subjective decision-making processes based on multiple attributes in a hierarchical system (Tzeng and Huang 2011). In the AHP method, a decision problem is considered as a hierarchical structure and, according to their properties, it is decomposed into elements and

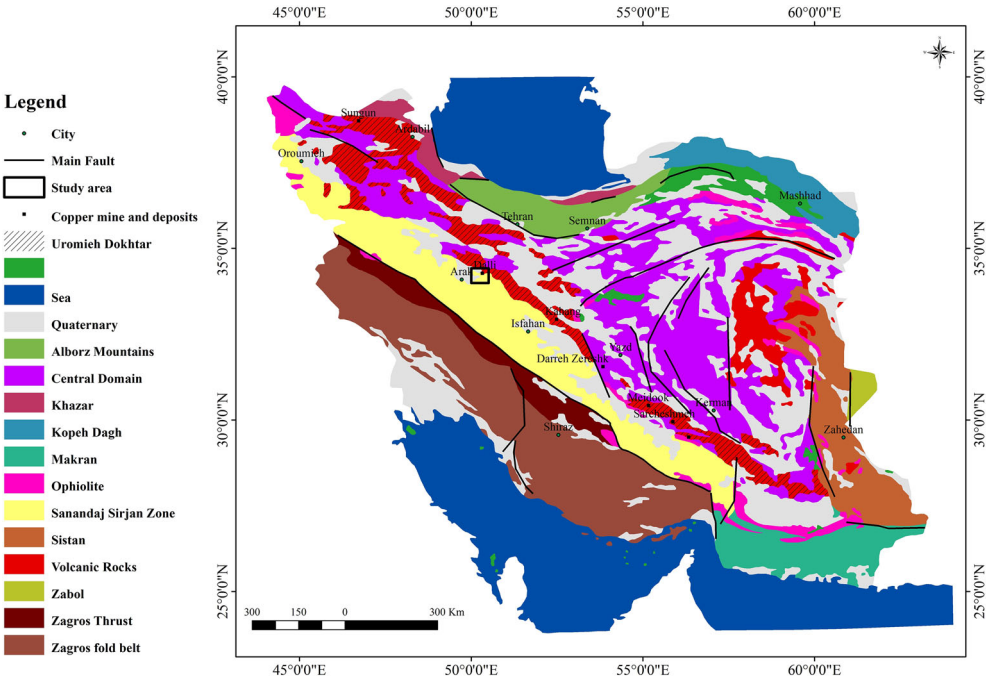

Figure 1. Generalized geologic map of Iran (modified after Aghanabati (2004) and location of study area.

levels corresponding to the common characteristic of the elements. The first level is the final goal of the problem, and the intermediate levels correspond to criteria and sub-criteria, while the lowest level contains the decision alternatives.

The elements of each level are compared pairwise to a specific element in the immediate upper level. Table 1 shows the pairwise comparison scale of real numbers from 1 to 9 used in the AHP that was first developed by Saaty (1977). It allows converting the qualitative judgments into numerical values with intangible attributes.

The pairwise comparison matrix for "n" criteria $\{c_1, c_2, c_3, \ldots, c_n\}$ in the second level, with respect to the final goal, is formed as

$$A = \begin{bmatrix} a_{11} & a_{12} & \cdots & a_{1n} \\ a_{21} & a_{22} & \cdots & a_{2n} \\ \cdots & \cdots & \cdots & \cdots \\ a_{n1} & a_{n2} & \cdots & a_{nn} \end{bmatrix},$$

where a_{ij} represents the pairwise comparison rating between the elements i and j of a level with respect to the upper level. The entries a_{ij} are governed by the following rules:

$$a_{ij} > 0; \quad a_{ij} = 1/a_{ji}; \quad a_{ii} = 1 \; \forall \; i.$$

There are some simple methods for calculating the weight vector from the pairwise comparison matrix A, and the eigenvalue approach proposed by Saaty (1977, 1980) is one of them. Based on the eigenvalue approach (Saaty 1980, 2000), the weight vector can be estimated by finding the principal eigenvector w of the matrix A, thus

$$Aw = \lambda_{\max} w.$$

When the vector w is normalized, it becomes the weight vector of elements of one level with respect to the upper level. $\lambda_{\max}$ is the largest eigenvalue of the matrix A. In cases where the pairwise comparison matrix satisfies transitivity for all pairwise comparisons, it is said to be consistent and it verifies the following relation:

$$a_{ij} = a_{ik} \times a_{kj}; \quad \forall i, \; j, \; k.$$

Saaty (1980) has shown that to maintain reasonable consistency when deriving weight vector from paired comparisons, the number of factors being considered must be less than or equal to nine. AHP allows inconsistency, but provides a measure of the inconsistency in each set of judgments. The consistency of the judgmental matrix can be determined by a measure called the consistency ratio (CR), defined as

Table 1. Ratio scales in AHP method (from Saaty 1977)

Intensity	1	3	5	7	9	2, 4, 6, 8
Linguistic	Equal	Moderate	Strong	Demonstrated	Extreme	Intermediate value

$$\mathrm{CR} = \frac{\mathrm{CI}}{\mathrm{RI}},$$

where CI is called the consistency index and RI is the random index. Furthermore, Saaty (1980, 2000) provided average consistencies (RI values) of randomly generated matrices (Table 2). The CI for a matrix of order n is defined as

$$\mathrm{CR} = \frac{\lambda_{\max} - n}{n-1}.$$

In general, a consistency ratio of 0.1 or less is considered acceptable. If the value is higher, the judgments may not be reliable and should be elicited again.

TOPSIS

TOPSIS is a well-known ranking method for MCDM that was proposed by Hwang and Yoon (1981), and then developed by Lai et al. (1994) and Yoon and Hwang (1995). The logic of the TOPSIS approach is to define ideal and anti-ideal solutions (Liang 1999), which are based on the concept of relative closeness in compliance with that the shorter (or longer) the distance of an alternative to ideal (or anti-ideal), the higher the priority ranking (Zeleny 1982).

On the basis of many criteria to rank, various situations are evaluated and compared for the MCDM problems. Therefore, a set of alternatives $A = \{a, b, c,\ldots\}$ are evaluated by n criteria $C = \{c_1, c_2, c_3,\ldots\}$ and the aim is to find the best alternative in the set of A based on the comparison of criterion vector C.

TOPSIS has a simple algorithm with attractive property in that limited subjective input is needed from decision makers (Jahanshahloo et al. 2006; Tzeng and Huang 2011; Opricovic and Tzeng 2004). The only subjective input needed is weights (Olson 2004), which, in this paper, are determined by AHP method. The procedure of TOPSIS can be summarized in the following simple steps (Hwang and Yoon 1981; Jahanshahloo et al. 2006; Tzeng and Huang 2011):

(1) Establish a decision matrix for the ranking. The structure of the matrix can be expressed as follows:

$$D = \begin{array}{c} \\ A1 \\ A2 \\ . \\ . \\ Ai \\ . \\ Am \end{array} \begin{array}{c} \begin{array}{ccccccc} c_1 & c_2 & & c_j & & c_n \end{array} \\ \begin{bmatrix} g_{11} & g_{12} & \cdots & g_{1j} & \cdots & g_{1n} \\ g_{21} & g_{22} & \cdots & g_{2j} & \cdots & g_{2n} \\ . & . & \cdots & . & \cdots & . \\ . & . & \cdots & . & \cdots & . \\ g_{i1} & g_{i2} & \cdots & g_{ij} & \cdots & g_{in} \\ . & . & \cdots & . & \cdots & . \\ g_{m1} & g_{m2} & \cdots & g_{mj} & \cdots & g_{mn} \end{bmatrix} \end{array}$$

where Ai denotes the alternatives i, $i = 1, 2, 3, \ldots, m$; c_j represents jth attribute or criterion, $j = 1, 2, \ldots, n$, related to ith alternative; and g_{ij} is a crisp value indicating the performance rating of each alternative A_i with respect to each criterion c_j.

(2) Calculate the normalized decision matrix. The normalized value r_{ij} is calculated as

$$r_{ij} = g_{ij} \Big/ \sqrt{\sum_{i=1}^{m} g_{ij}^2}; \quad i = 1,2,\ldots,m; \quad j = 1,2,\ldots,n.$$

(3) Calculate the weighted normalized decision matrix. The weighted normalized value v_{ij} is calculated as

$$v_{ij} = w_j r_{ij}; \quad i = 1,2,\ldots,m; \quad j = 1,2,\ldots,n,$$

where w_j is the weight of the ith attribute or criterion and $\sum_{j=1}^{n} w_j = 1$.

(4) Determine the positive ideal and negative ideal solutions.

$$A^* = \{v_1^*,\ldots,v_n^*\} = \{(\max_i v_{ij} | j \in J'),(\min_i v_{ij} | j \in J'')\}$$
$$A^- = \{v_1^-,\ldots,v_n^-\} = \{(\min_i v_{ij} | j \in J'),(\max_i v_{ij} | j \in J'')\},$$

where J' is the set of benefit criteria and J'' is the set of cost criteria.

Table 2. Values of *RI* for different matrix sizes (Tzeng and Huang 2011)

Number of elements	3	4	5	6	7	8	9	10	11	12	13
RI	0.52	0.89	1.11	1.25	1.35	1.4	1.45	1.49	1.51	1.54	1.56

(5) Calculate the separation measures using the *n*-dimensional Euclidean distance. The separation of each alternative from the ideal solution and negative ideal solution are given as

$$D_i^* = \sqrt{\sum_{j=1}^{n} (v_{ij} - v_j^*)^2}; \quad i = 1, 2, \ldots, m.$$

$$D_i^- = \sqrt{\sum_{j=1}^{n} (v_{ij} - v_j^-)^2}; \quad i = 1, 2, \ldots, m.$$

(6) Calculate the relative closeness to the ideal solution. The relative closeness of the alternative A_i with respect to A^* is defined as

$$\mathrm{RC} = \frac{D_i^-}{(D_i^- + D_i^*)}, \quad i = 1, 2, \ldots, m.$$

(7) Ranking the alternative based on relative closeness.

The best alternative is the one that has the higher *RC*. By sorting the calculated relative closeness, the best alternatives are ranked.

MINERAL POTENTIAL TARGETING ELEMENTS

Genetic and spatial information from the known Dalli porphyry Cu–Au deposit of the study area as well as information from typical porphyry Cu–Au genetic modeling was used to identify the targeting elements (exploration criteria) for district-scale exploration in the Salafchegan area (Table 3).

Two sets of characteristics were defined from the generic Cu–Au porphyry deposit models and the Dalli deposit and conjunctively used to recognize the key targeting elements for district-scale exploration of Cu–Au porphyry mineralization in the Salafchegan area. These characteristics are as follows: (1) host lithologies of Miocene diorite, quartz-diorite to granodiorite intrusions and their contact with Eocene andesite porphyry; (2) silicic, potassic, and phyllic hydrothermal alterations surrounded by argillic and propylitic alterations; (3) ferric iron oxides of mostly hematite and goethite; (4) strong copper and gold geochemical anomalies associated with arsenic, iron, and potassium; (5) strong magnetic signatures associated with the host intrusions and mineralized potassic alterations; and (6) NE–SW trending structures.

Then, the geological map (1:100,000 scale), and Enhanced Thematic Mapper (ETM+) and Advanced Spaceborne Thermal Infrared (ASTER) satellite imagery data, as well as geochemical, geophysical, and field data were utilized to search for the above-mentioned porphyry Cu–Au targeting elements.

Lithology

A wide range of igneous rocks are host to porphyry Cu (Au, Mo) mineralization. Singer et al. (2005, 2008) compiled the host rocks of 407 porphyry copper deposits and indicated that intermediate intrusive rocks are the most important and frequent hosts to porphyry Cu (Au, Mo) mineralization (Fig. 2).

Mineralization at Dalli is hosted by altered Miocene intermediate intrusive rocks, such as quartz-diorite, that intruded Eocene andesite porphyry. High-grade mineralization occurs at the contact of the quartz-diorite intrusion and andesite porphyry. A northeast-trending structural corridor provided the favorable site for porphyry intrusion and pathway for mineralizing hydrothermal solutions. The alteration system covers an area of 20 km^2 and mostly comprises mineralized potassic and phyllic alterations, surrounded by extensive barren argillic (kaolinite) and propylitic (chlorite) alterations (Ayati et al. 2013).

Based on the above-mentioned information, the 1:100,000 scale geological map of the study area was reclassified into eight lithological classes. Some of these classes are favorable hosts to porphyry Cu–Au mineralization. Figure 3 shows the reclassified geological map of the area overlain by the known porphyry occurrences.

Table 3. Characteristics of Dalli Cu–Au porphyry deposit compared with typical Cu–Au porphyry deposits

Characteristic features	Typical porphyry Cu–Au mineralization (Halter et al. 2004; Sillitoe 2010; Richards and Mumin 2013)	Dalli porphyry Cu–Au deposit (Asadi 2008; Ayati et al. 2008; John et al. 2010; Ayati et al. 2013)
Geodynamic setting	Subduction and post-subduction	Subduction, continental volcanic arc
Host rock	Diorite to granodiorite	Miocene diorite to quartz-diorite intrusions and their contacts with Eocene andesite porphyry
Magmatic association	Calc-alkaline to mildly alkaline; intermediate to felsic intrusion	Calc-alkaline intermediate to felsic intrusion
Source of fluids	Magmatic	Magmatic
Hydrothermal alteration	Potassic, siliceous, and propylitic (±phyllic and argillic)	K-feldspar, secondary biotite, silica, sericite surrounded by kaolinite, chlorite, and epidote
Mineralogy	Chalcopyrite, bornite, magnetite; native gold abundant pyrite with K-feldspar and sericite	Magnetite, specular hematite, goethite, chalcopyrite, malachite, bornite, chalcocite, native gold, and native copper
Element association	Cu–Au–Ag–Fe–Sn–W–K–Mo–Na–S–SiO_2	Cu–Au–Fe–As, K–(Na)–S–SiO_2
Structural controls	Transpression or transtension	NE–SW trending extensional faults (up to 1.5-km-wide structural corridors
Original depth of mineralization (km)	1–5	3–4
Age	Dominant in phanerozoic	17–20 Ma (Miocene

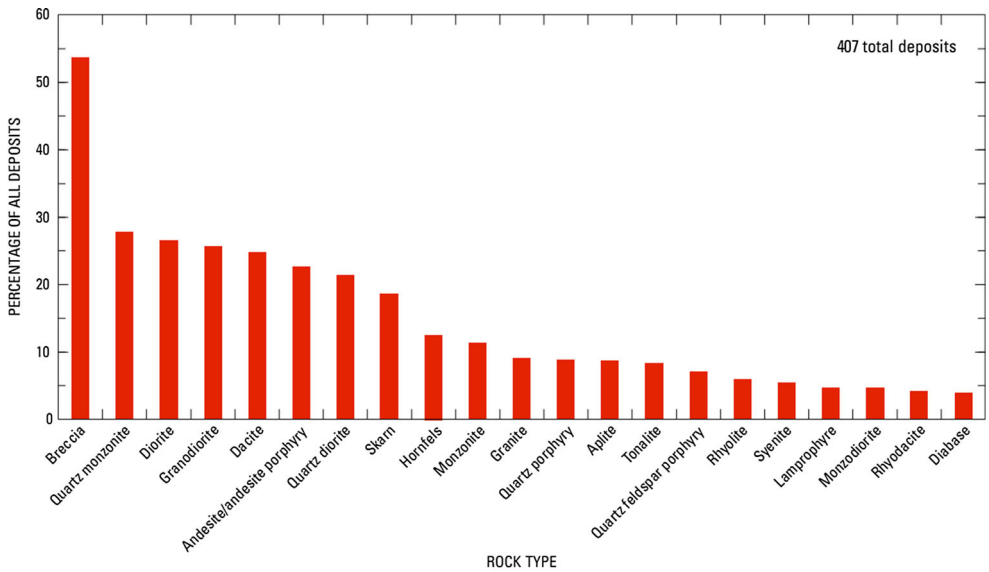

Histogram of rock types in porphyry copper deposits based on compilation by Singer and others (2008).

Figure 2. Histogram of major host rocks of porphyry Cu (Au, Mo) deposits (Singer et al. 2005, 2008).

Structures

Structures provide pathways for mineralizing fluids and porous zones for trapping metals. Faults, extracted from the 1:100,000 scale geological map of the study area, were used to prepare a lineament density raster map with a grid-cell size of 100 m (Fig. 4). The known porphyry Cu–Au deposits/prospects of the study area (e.g., Dalli and Zavarian) occur in zones with moderate lineament density (Fig. 4).

Hydrothermal Alteration

Hydrothermal alterations and iron oxides are important distal or direct features in porphyry Cu–Au exploration. In recent years, ASTER and

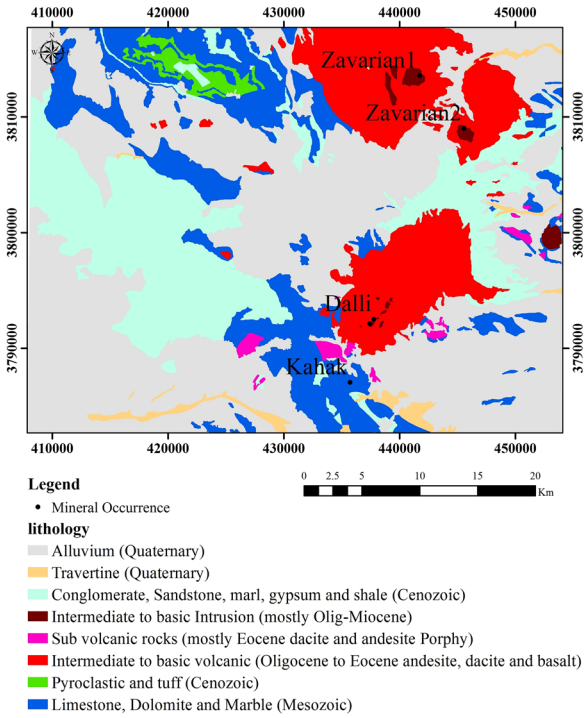

Figure 3. Reclassified geological map of the study area.

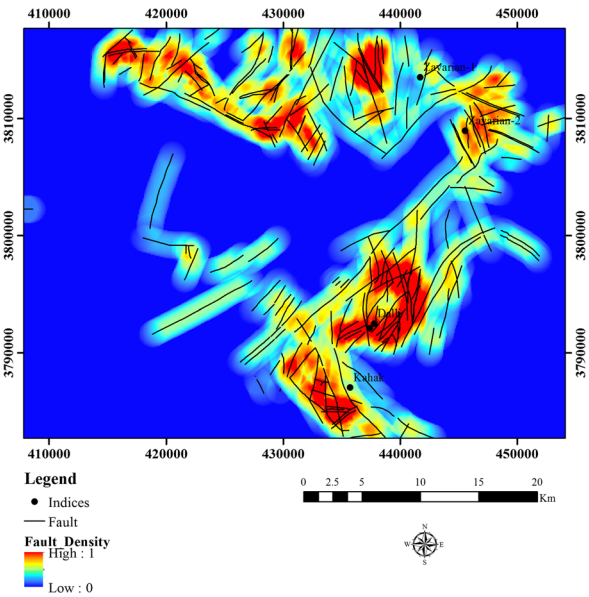

Figure 4. Lineament density map of the Salafchegan area.

ETM+ satellite imagery data have been extensively used for mapping alterations (Abrams et al. 1983; Amos and Greenbaum 1989; Sabins 1999; Galvao et al. 2005; Rowan et al. 2005; Gabr et al. 2010; Pour et al. 2011, Honarmand et al. 2012; Pour and Hashim 2012; Feizi and Mansuri 2013; Shahriari et al. 2013; Pournamdari et al. 2014; Shahriari et al. 2014). The main hydrothermal alterations associated with Dalli and other typical porphyry Cu–Au deposits are potassic, silica, hydroxyl-bearing clay, phyllic, and propylitic alterations. Iron oxides, closely associated with these alterations, are also important features of interest in porphyry Cu–Au exploration.

Spectral angle mapper (SAM) (Kruse et al. 1993) and Least Square Fit (Ls-Fit) methods were applied to ASTER and ETM+ satellite imagery data to map hydrothermal alterations and iron oxides. Hydroxyl clay minerals such as kaolinite (argillic alteration) and iron oxides were mapped from Landsat ETM+ data using the LS-Fit method, while chlorite and silicification were mapped from ASTER data using the SAM method. The hydrothermal alterations including silicification, OH-bearing clays, and chlorite were combined with mapped iron oxides to be used as an important input map in the data integration modeling (Fig. 5).

Geochemistry

A sample catchment basin analysis (CBA) was conducted using stream sediment geochemical data in the study area to generate geochemical anomalies associated with copper mineralization. Two hundred fifty stream sediment samples were collected and analyzed for 12 elements by the Geological Survey of Iran using ICP method at Zar Azma and Kan Pajuh laboratories in Iran. The samples were analyzed for Cu among those 12 elements, but not for gold or other important elements associated with Cu–Au mineralization of the study area. Therefore, we only used the Cu analytical results for mapping stream sediment geochemical anomalies for data integration modeling. To obtain a raster map of Cu anomaly, catchment basins were prepared using the locations of stream sediment samples and digital elevation model of the area. Then, the Cu concentration of each sample is assigned to its related catchment basin. Dalli and Zavarian and their surrounding areas show strong catchment basin Cu anomalies (Fig. 6).

Magnetic Features

Magnetic data have been widely used to map porphyry intrusive rocks, structures, and hydrother-

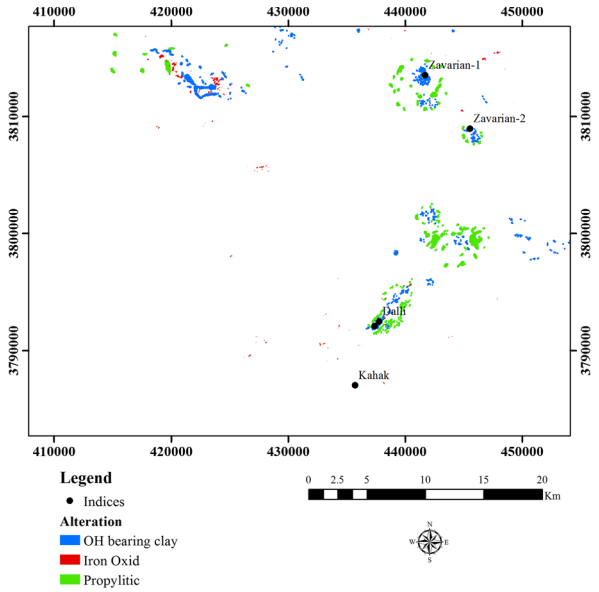

Figure 5. Hydrothermal alterations and iron oxides mapped from Landsat ETM$^+$ and ASTER data.

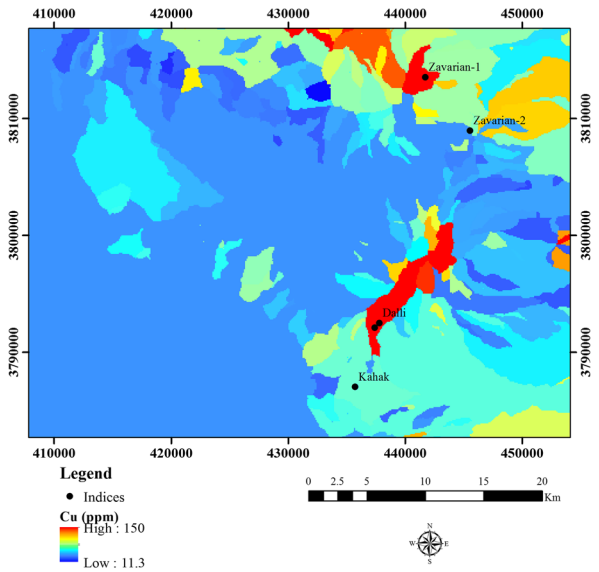

Figure 6. Sample catchment basin geochemical Cu map.

mal alterations in porphyry Cu–Au exploration (Thoman et al. 2000, Holden et al. 2011; Abedi et al. 2013). According to Clark (2014), induced magnetic anomalies, caused by Au-rich porphyry Cu systems, have specific semi-predictable characteristics. A magnetic intrusion and the associated magnetite-bearing potassic alteration zone, typically create a circular positive magnetic anomaly. This sub-circular magnetic high is surrounded by an annular negative magnetic anomaly caused by propylitic and phyllic alteration zones. This negative magnetic anomaly is caused by destruction of magnetite in the volcanic country rock. The distinctive circular magnetic peak at its center contrasts sharply with the surrounding zones (Holden et al. 2011). Therefore, high-amplitude magnetic anomalies are expected to occur in porphyry intrusive rocks and potassic alteration in the porphyry Cu–Au deposits.

Recently, Holden et al. (2011) proposed an automatic circular feature extraction to enhance the magnetic anomalies related to porphyry copper deposits. On the other hand, derivative-based methods have been used for many years in magnetic data interpretation. In this paper, we used the tilt angle method as a tool for enhancing the magnetic anomalies, associated with porphyry intrusive rocks (Miller and Singh 1994; Verduzco et al. 2004). The tilt angle, T, is a useful filter for enhancing subtle anomalies in potential field data and was first proposed by Miller and Singh (1994) as

$$T = \tan^{-1}\left[\frac{\partial M}{\partial z} \Big/ \sqrt{\left(\frac{\partial M}{\partial x}\right)^2 + \left(\frac{\partial M}{\partial y}\right)^2}\right],$$

where $\frac{\partial M}{\partial x}$, $\frac{\partial M}{\partial y}$, and $\frac{\partial M}{\partial z}$ are the first-order derivatives of the magnetic field M in the x, y, and z directions, respectively. The tilt angle has many interesting properties, for example, due to the nature of the arctan trigonometric function, all tilt amplitudes are restricted to values between $-90°$ and $+90°$ regardless of the amplitude of the vertical or the absolute value of the total horizontal gradient (Salem et al. 2007). The positive values are located on the magnetic body and zero value along its boundary. This method can also be applied to the reduced-to-the-pole (RTP) magnetic map. In the RTP map, the inclination effect of magnetic field is corrected and high values are located on the magnetic body, while in the total magnetic intensity map magnetic sources show a dipolar anomaly and maximum values have a distance with the center of the mass.

In this study, the aeromagnetic data were extracted from the nation-wide airborne magnetic data of Iran (flight-line spacing of 7.5 km). Figure 7 shows the RTP and tilt angle maps of the study area. The tilt angle map highlighted positive magnetic anomalies that can be related to porphyry intrusive rocks associated with porphyry Cu–Au mineralization (Fig. 7).

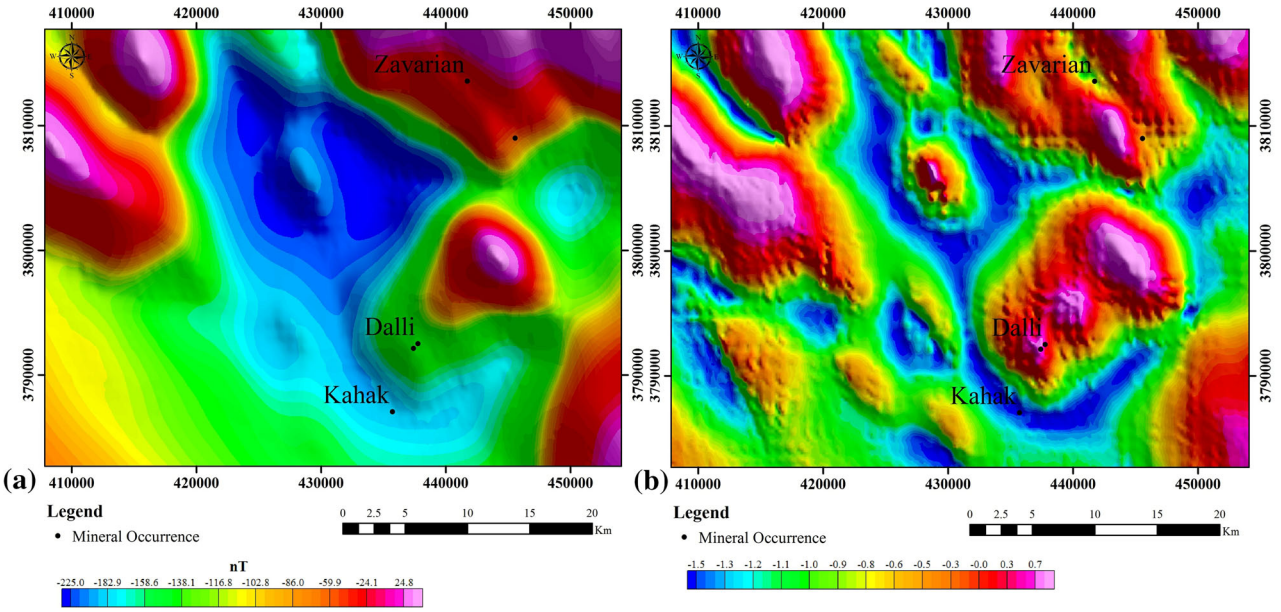

Figure 7. Reduced-to-the-pole (RTP) magnetic map (*left*) and tilt angle of RTP magnetic data (*right*).

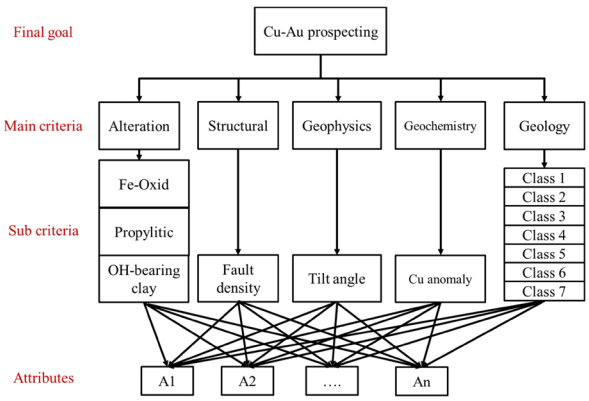

Figure 8. Hierarchical structure for mapping the porphyry Cu–Au potential of the study area. Geology classes are described in Table 4. Each pixel has attributes A1 to An.

DATA INTEGRATION MODELING

An integrated AHP–TOPSIS method was used to combine the input exploration data and create a final porphyry Cu–Au prospectivity map of the Salafchegan area. First, a hierarchy structure for porphyry Cu–Au exploration in the study area was designed using the input exploration maps (Fig. 8). Then, a pairwise comparison matrix was created and five input criteria were compared to indicate porphyry Cu–Au potential of the area. On the basis of the calculated weights, the relative importance of each of the criteria with respect to the porphyry Cu–Au potential is shown in Table 4. The criteria weight vector was calculated from the pairwise comparison matrix and the AHP method. The consistency ratio for this pairwise comparison is CR = 0.017 which is less than 0.1 and thus this value is acceptable (Tzeng and Huang 2011).

The geological and alteration criteria have some sub-criteria that their relative weights must be determined. The geological criterion consists of seven sub-criteria (lithological units). The comparison matrix for the lithological units with respect to the geological criterion was prepared using the targeting elements generated from the Dalli Cu–Au porphyry deposit and generic porphyry Cu–Au deposit models (Table 3). Then, the weights for the seven lithological classes were calculated using the AHP method (Table 5).

The alteration criterion has three sub-criteria including the iron oxides, OH-bearing clay, and propylitic alterations. The relative weights of these alteration sub-criteria were also calculated using the AHP method (Table 6).

For applying the proposed AHP–TOPSIS algorithm, cell values of raster maps associated with the five criteria and lithological and alteration sub-criteria were extracted to make a decision matrix. Using the developed MATLAB codes for the proposed AHP–TOPSIS method, the relative closeness

Table 4. Pairwise comparison matrix of the main criteria used for mapping porphyry Cu–Au potential

Criteria	Alteration	Structure	Geology	Geochemistry	Geophysics	Weights
Alteration	1	2	3	1/2	5	0.27
Structure	1/2	1	2	1/3	4	0.16
Geology	1/3	1/2	1	1/4	3	0.1
Geochemistry	2	4	4	1	7	0.42
Geophysics	1/5	1/4	1/3	1/7	1	0.05
CR = 0.017						

Table 5. Comparison matrix of the weights for the seven lithological classes estimated using the AHP

Lithologies	Class 1	Class 2	Class 3	Class 4	Class 5	Class 6	Class 7	Weights
Class 1: intermediate to basic intrusions	1	2	3	4	6	7	9	0.35
Class 2: sub-volcanics (e.g., andesite and dacite porphyry)	1/2	1	2	3	5	6	7	0.24
Class 3: intermediate to basic volcanics (e.g., andesite and basalt)	1/3	1/2	1	3	5	6	7	0.19
Class 4: pyroclastic and tuffs	1/4	1/3	1/3	1	3	5	6	0.11
Class 5: carbonate rocks	1/6	1/5	0.2	1/3	1	3	5	0.06
Class 6: conglomerate, sandstone, marl, and shale	1/7	1/6	1/6	0.2	1/3	1	3	0.03
Class 7: alluvium	1/9	1/7	1/7	1/6	0.2	1/3	1	0.02
CR = 0.065								

Table 6. Comparison matrix of weights for the alteration sub-criteria estimated using AHP

Alterations	Iron oxide	OH-bearing clay	Propylitic	Weights
Iron oxide	1	2	3	0.54
OH-bearing clay	1/2	1	3/2	0.27
Propylitic	1/3	2/3	1	0.19
CR = 0.033				

to the ideal solution for each alternative (cell pixels) was calculated.

A final porphyry Cu–Au prospectivity map was created and reclassified into three classes. The thresholds for classification of favorability map were determined using the favorability—area fractal modeling in a similar way to concentration—area fractal modeling mentioned in literatures (Agterberg 1995; Cheng 1999; Carranza 2009). Figure 9 shows the log–log plot of fractal result, which indicates three straight lines with breaks in C1 and C2 that are considered as thresholds for classification. Figure 10 shows the porphyry Cu–Au prospectivity map, which accurately depicts the prominent porphyry Cu–Au mineralized zones (Dalli and Zavarian) to be located in the high favorability class. In addition, an area with high potential (similar to Dalli

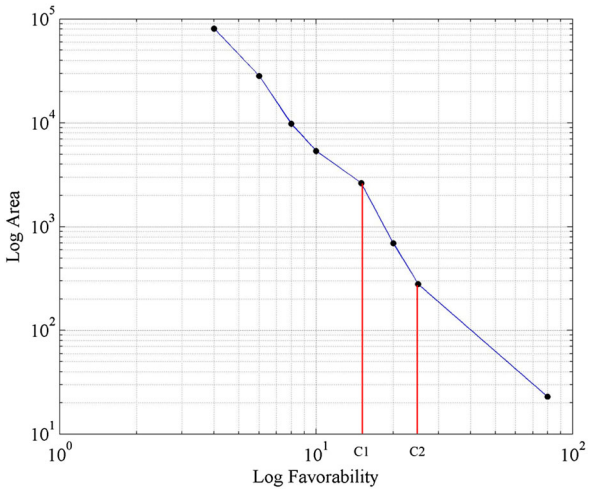

Figure 9. Log–log plot of favorability area.

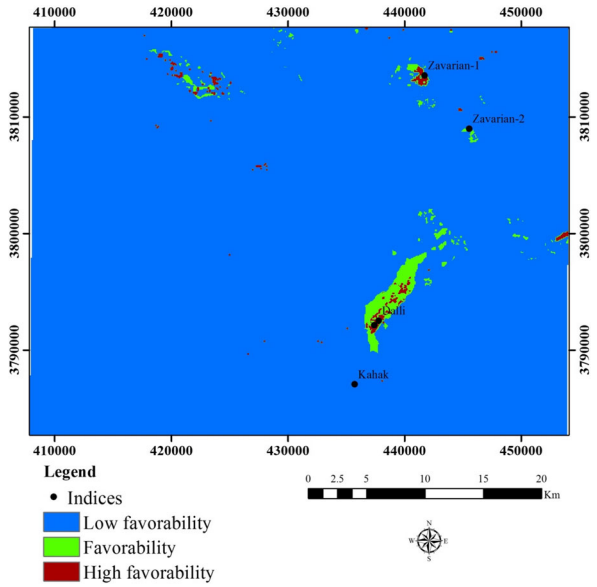

Figure 10. Favorability map obtained from the combination of various geoscience datasets through the integrated AHP–TOPSIS method.

and Zavarian porphyry Cu–Au mineralized areas) was determined in the northwest of the area. This area needs follow-up exploration.

DISCUSSION AND CONCLUSION

In this paper, an innovative data integration approach based on an MCDM method (i.e., the integrated AHP–TOPSIS) is proposed for mineral potential mapping. This method is based on the two most popular MCDM algorithms known as AHP and TOPSIS. In this algorithm, the criteria weight vector is obtained based on the pairwise comparison matrix and AHP algorithm and the alternatives are ranked by TOPSIS. The pairwise comparison matrix is prepared by expertise in porphyry Cu–Au potential mapping. After that, the alternatives (the raster map pixels) are ranked by the TOPSIS algorithm. This strategy has some similarity to both data-driven and knowledge-driven algorithms. It needs a criteria weight vector as a knowledge-driven algorithm, but it does not employ an inference system as in knowledge-driven methods (e.g., fuzzy logic). The ranking strategy is only based on the distance of alternatives to positive and negative ideals, similar to the fuzzy c-means clustering (for two clusters) whereby the similarity of each alternative is measured by comparison to cluster prototypes (the prototypes of clusters are positive and negative ideal solutions). Therefore, the proposed method is not a pure knowledge- or data-driven method, but is a hybrid method. The proposed algorithm only needs the comparison matrix as primary information for obtaining the criteria weight vector, whereas other knowledge-driven methods, such as fuzzy logic, need more primary information of the membership function for fuzzification of input data in addition to criteria weight vector.

The AHP–TOPSIS algorithm was used for integrating datasets from a greenfield area with very few known deposits in the central part of Urumieh–Dokhtar magmatic arc, the main volcanic arc and porphyry copper belt of Iran. Five exploration layers (hydrothermal alterations, structural features, catchment basin geochemical anomaly map of copper, total magnetic intensity map of airborne data, and 1:1000000 scale lithological map) of the study area were prepared and integrated to create a final favorability map. On the basis of the fractal method, the final favorability map was classified as three classes of high favorable, favorable, and low favorable zones. The high favorable classes cover about 0.05 percent of the study area and contain the three known prominent deposits, namely Dalli south and Dalli north porphyry Cu–Au deposits and the Zavarian 1 porphyry Cu–Au prospect. The favorable classes cover about 1.5 percent of the study area and Zavarian 2 porphyry Cu–Au prospect locates in these classes. Kahak, which is an iron-skarn deposit, lies in the low favorable class. Several unknown high favorable and favorable areas are now recognized northeast of the Dalli deposits and east of the Zavarian deposits. Follow-up exploration of these high-potential areas is recommended.

REFERENCES

Abedi, M., & Norouzi, G. H. (2012). Integration of various geophysical data with geological and geochemical data to determine additional drilling for copper exploration. *Journal of Applied Geophysics, 83*, 35–45.

Abedi, M., Norouzi, G. H., & Bahroudi, A. (2012a). Support vector machine for multi-classification of mineral prospectivity areas. *Computers & Geosciences, 46*, 272–283.

Abedi, M., Norouzi, G. H., & Fathianpour, N. (2013). Fuzzy outranking approach: A knowledge-driven method for mineral prospectivity mapping. *International Journal of Applied Earth Observation and Geoinformation, 21*, 556–567.

Abedi, M., Norouzi, G. H., & Torabi, S. A. (2012b). Clustering of mineral prospectivity area as an unsupervised classification

approach to explore Copper Deposit. *Arabian Journal of Geosciences, 6*, 3601–3613.
Abedi, M., Torabi, S. A., Norouzi, G. H., & Hamzeh, M. (2012c). ELECTRE III: A knowledge-driven method for integration of geophysical data with geological and geochemical data in mineral prospectivity mapping. *Journal of Applied Geophysics, 87*, 9–18.
Abedi, M., Torabi, S. A., Norouzi, G. H., Hamzeh, M., & Elyasi, G. R. (2012d). PROMETHEE II: A knowledge-driven method for copper exploration. *Computers & Geosciences, 46*, 255–263.
Abrams, M. J., Brown, D., Lepley, L., & Sadowski, R. (1983). Remote sensing for porphyry copper deposits in southern Arizona. *Economic Geology, 78*, 591–604.
Aghanabati, A. (2004). *Geology of Iran*. Geological Survey of Iran: Ministry of industry and mines. **582 p**.
Agterberg, F. P. (1995). Multifractal modeling of the sizes and grades of giant and supergiant deposits. *International Geology Reviews, 37*, 1–8.
Amos, B. J., & Greenbaum, D. (1989). Alteration detection using TM imagery: The effects of supergene weathering in arid climate. *International Journal of Remote Sensing, 10*, 515–527.
An, P., Moon, W. M., & Rencz, A. (1991). Application of fuzzy set theory for integration of geological, geophysical and remote sensing data. *Canadian Journal of Exploration Geophysics, 27*, 1–11.
Asadi, H.H. (2008). Final exploration report of Dalli porphyry Cu–Au deposit, Markazi province. Technical report. Dorsa Pardazeh Company.
Asadi, H. H., & Hale, M. (2001). A predictive GIS model for mapping potential gold and base metal mineralization in Takab area, Iran. *Computers & Geosciences, 27*, 901–912.
Asadi, H. H., Porwal, A., Fatehi, M., Kianpouryan, S., & Lu, Y. J. (2015). Exploration feature selection applied to hybrid data integration modeling: Targeting copper-gold potential in central Iran. *Ore Geology Reviews, 71*, 819–838.
Ayati, F., Yavuz, F., Asadi, H. H., Richards, J. P., & Jourdan, F. (2013). Petrology and geochemistry of calc-alkaline volcanic and subvolcanic rocks, Dalli porphyry copper–gold deposit, Markazi Province, Iran. *International Geology Reviews, 55*, 158–184.
Ayati, F., Yavuz, F., Noghreyan, M., Asadi, H. H., & Yavuz, R. (2008). Chemical characteristics and composition of hydrothermal biotite from the Dalli porphyry copper prospect, Arak, central province of Iran. *Mineralogy and Petrology, 94*, 107–122.
Bonham-Carter, G. F. (1994). *Geographic information systems for geoscientists: Modelling with GIS* (p. 398). Oxford: Pergamon Press.
Bonham-Carter, G. F., Agterberg, F. P., & Wright, D. F. (1989). Weights-of-evidence modelling: A new approach to mapping mineral potential. In F. P. Agterberg & G. F. Bonham-Carter (Eds.), *Statistical applications in the earth sciences* (pp. 171–183). Ottawa: Geological Survey of Canada.
Carranza, E. J. M. (2009). *Geochemical anomaly and mineral prospectivity mapping in GIS. Handbook of Exploration and Environmental Geochemistry 11*. New York: Elsevier.
Carranza, E. J. M. (2011). Geocomputation of mineral exploration targets. *Computers & Geosciences, 37*, 1907–1916.
Carranza, E. J. M., Hale, M., & Faassen, C. (2008). Selection of coherent deposit-type locations and their application in data-driven mineral prospectivity mapping. *Ore Geology Reviews, 33*, 536–558.
Carranza, E. J. M., & Laborte, A. G. (2015a). Data-driven predictive mapping of gold prospectivity, Baguio district, Philippines: Application of Random Forests algorithm. *Ore Geology Reviews, 71*, 777–787.
Carranza, E. J. M., & Laborte, A. G. (2015b). Data-driven predictive modeling of mineral prospectivity using Random Forests: A case study in Catanduanes Island (Philippines). *Natural Resources Research*. doi:10.1007/s11053-015-9268-x.
Carranza, E. J. M., & Laborte, A. G. (2015c). Random forest predictive modeling of mineral prospectivity with small number of prospects and data with missing values in Abra (Philippines). *Computers & Geosciences, 74*, 60–70.
Carranza, E. J. M., Mangaoang, J. C., & Hale, M. (1999). Application of mineral deposit models and GIS to generate mineral potential maps as input for optimum land-use planning in the Philippines. *Natural Resources Research, 8*, 165–173.
Cheng, Q. (1999). Spatial and scaling modeling for geochemical anomaly separation. *Journal of Geochemical Exploration, 65*, 175–194.
Clark, D. A. (2014). Magnetic effects of hydrothermal alteration in porphyry copper and iron-oxide copper–gold systems: A review. *Tectonophysics, 624–625*, 46–65.
Feizi, F., & Mansuri, E. (2013). Separation of alteration zones on ASTER data and integration with drainage geochemical maps in Soltanieh, Northern Iran. *Open Journal of Geology, 3*, 134–142.
Ford, A., Miller, J. M., & Mol, A. G. (2015). A comparative analysis of weights of evidence, evidential belief functions, and fuzzy logic for mineral potential mapping using incomplete data at the scale of investigation. *Natural Resources Research*. doi:10.1007/s11053-015-9263-2.
Gabr, S., Ghulam, A., & Kusky, T. (2010). Detecting areas of high-potential gold mineralization using ASTER data. *Ore Geology Reviews*, *38*, 59–69.
Galvao, L. S., Filho, R. A., & Vitorello, I. (2005). Spectral discrimination of hydrothermally altered materials using ASTER short-wave infrared bands: Evaluation in a tropical savannah environment. *International Journal of Applied Earth Observation and Geoinformation, 7*, 107–114.
Geranian, H., Tabatabaei, S. H., Asadi, H. H., & Carranza, E. J. M. (2015). Application of discriminant analysis and support vector machine in mapping gold potential areas for further drilling in the Sari-Gunay gold deposit, NW Iran. *Natural Resources Research*. doi:10.1007/s11053-015-9271-2.
Halter, W. E., Bain, N., Becker, K., Heinrich, C. A., Landtwing, M., VonQuadt, A., et al. (2004). From andesitic volcanism to the formation of a porphyry Cu–Au mineralizing magma chamber: The Farallo'n Negro Volcanic Complex, northwestern Argentina. *Journal of Volcanology and Geothermal Research, 136*, 1–30.
Holden, E. J., Fu, S. C., Kovesi, P., Dentith, M., Bourne, B., & Hope, M. (2011). Automatic identification of responses from porphyry intrusive systems within magnetic data using image analysis. *Journal of Applied Geophysics, 74*, 255–262.
Honarmand, M., Ranjbar, H., & Shahabpour, J. (2012). Application of principal component analysis and spectral angle mapper in the mapping of hydrothermal alteration in the Jebal-Barez Area, Southeastern Iran. *Resource Geology, 62*, 119–139.
Hosseinali, F., & Alesheikh, A. A. (2008). Weighting spatial information in GIS for copper mining exploration. *American Journal of Applied Sciences, 5*(9), 1187–1198.
Hwang, C. L., & Yoon, K. (1981). *Multiple attribute decision making: Methods and applications*. New York: Springer.
Jahanshahloo, G. R., Hosseinzadeh Lotfi, F., & Izadikhah, M. (2006). An algorithmic method to extend TOPSIS for decision-making problems with interval data. *Applied Mathematics and Computation, 175*, 1375–1384.
John, D. A., Ayuso, R. A., Barton, M. D., Blakely, R. J., Bodnar, R. J., Dilles, J. H., Gray, F., Graybeal, F. T., Mars, J. C., McPhee, D. K., Seal, R. R., Taylor, R. D., & Vikre, P. G. (2010). Porphyry copper deposit model, chapter B of mineral deposit models for resource assessment. U.S. Geological Survey Scientific Investigations Report 2010–5070–B.

Kruse, F. A., Boardman, J. W., Lefkoff, A. B., Heidebrecht, K. B., Shapiro, A. T., Barloon, P. J., & Goetz, A. F. H. (1993). The spectral image processing system (SIPS)—interactive visualization and analysis of imaging spectrometer data. *Remote Sensing of the Environment, 44*, 145–163.

Lai, Y. J., Liu, T. Y., & Hwang, C. L. (1994). TOPSIS for MODM. *European Journal of Operational Research, 76*, 486–500.

Liang, G. S. (1999). Fuzzy MCDM based on ideal and anti-ideal concepts. *European Journal of Operational Research, 112*, 682–691.

McKay, G., & Harris, J. R. (2015). Comparison of the data-driven Random Forests model and a knowledge-driven method for mineral prospectivity mapping: A case study for gold deposits around the Huritz Group and Nueltin Suite, Nunavut, Canada. *Natural Resources Research*. doi:10.1007/s11053-015-9274-z.

Miller, H. G., & Singh, V. (1994). Potential field tilt—a new concept for location of potential field sources. *Journal of Applied Geophysics, 32*, 213–217.

Olson, D. L. (2004). Comparison of weights in TOPSIS models. *Mathematical and Computer Modelling*, *40*(7–8), 721–727.

Opricovic, S., & Tzeng, G. H. (2004). Compromise solution by MCDM methods: A comparative analysis of VIKOR and TOPSIS. *European Journal of Operational Research*, *156*(2), 445–455.

Pan, G. C., & Harris, D. P. (2000). *Information synthesis for mineral exploration*. New York: Oxford University Press.

Pazand, K., & Hezarkhani, A. (2015). Porphyry Cu potential area selection using the combine AHP-TOPSIS methods: A case study in Siahrud area (NW, Iran). *Earth Science Informatics, 8*, 207–220.

Pazand, K., Hezarkhani, A., & Ataei, M. (2012). Using TOPSIS approaches for predictive porphyry Cu potential mapping: A case study in Ahar-Arasbaran area (NW, Iran). *Computers & Geosciences, 49*, 62–71.

Pazand, K., Hezarkhani, A., Ataei, M., & Ghanbari, Y. (2011). Combining AHP with GIS for predictive Cu porphyry potential mapping: A case study in Ahar area (NW, Iran). *Natural Resources Research, 20*, 251–262.

Porwal, A., Carranza, E. J. M., & Hale, M. (2003a). Knowledge driven and data-driven fuzzy models for predictive mineral potential mapping. *Natural Resources Research, 12*, 1–25.

Porwal, A., Carranza, E. J. M., & Hale, M. (2003b). Artificial neural networks for mineral–potential mapping: A case study from Aravalli Province, Western India. *Natural Resources Research, 12*, 156–171.

Porwal, A., Carranza, E. J. M., & Hale, M. (2004). A hybrid neuro-fuzzy model for mineral potential mapping. *Mathematical Geology, 36*, 803–826.

Pour, A. B., & Hashim, M. (2012). Identifying areas of high economic-potential copper mineralization using ASTER data in the Urumieh-Dokhtar Volcanic Belt. *Iran. Advances in Space Research, 49*, 753–769.

Pour, B. A., Hashim, M., & Marghany, M. (2011). Using spectral mapping techniques on short wave infrared bands of ASTER remote sensing data for alteration mineral mapping in SE Iran. *International Journal of the Physical Sciences, 6*, 917–929.

Pournamdari, M., Hashim, M., & Beiranvand Pour, M. (2014). Application of ASTER and Landsat TM Data for geological mapping of esfandagheh ophiolite complex, Southern Iran. *Resource Geology, 64*, 233–246.

Richards, J. P., & Mumin, A. (2013). Magmatic-hydrothermal processes within an evolving Earth: Iron oxide–copper–gold and porphyry Cu ± Mo ± Au deposits. *Geology, 41*, 767–770.

Rowan, L. C., Mars, J. C., & Simpson, C. J. (2005). Lithologic mapping of the Mordor N.T., Australia ultramafic complex by using the advanced spaceborne thermal emission and reflection radiometer (ASTER). *Remote Sensing of the Environment, 99*, 105–126.

Saaty, T. L. (1977). A scaling method for priorities in hierarchical. *Journal of Mathematical Psychology, 15*, 234–281.

Saaty, T. L. (1980). *The analytic hierarchy process, planning, priority setting, resource allocation*. New York: McGraw-Hill.

Saaty, T. L. (2000). *Fundamentals of decision making and priority theory with the analytic hierarchy process*. Pittsburg: RWS Publication.

Sabins, F. F. (1999). Remote sensing for mineral exploration. *Ore Geology Reviews, 14*, 157–183.

Salem, A., Williams, S., Fairhead, J. D., & Ravat, D. (2007). Tilt-depth method: A simple depth estimation method using first-order magnetic derivatives. *The Leading Edge, 26*, 1502–1505.

Shahriari, H., Ranjbar, H., & Honarmand, M. (2013). Image segmentation for hydrothermal alteration mapping using PCA and concentration-area fractal model. *Natural Resources Research, 22*, 191–206.

Shahriari, H., Ranjbar, H., Honarmand, M., & Carranza, E. J. M. (2014). Selection of less biased threshold angles for SAM classification using the real value–area fractal technique. *Resource Geology, 64*, 301–315.

Sillitoe, R. H. (2010). Porphyry copper systems. *Economic Geology, 105*, 3–41.

Singer, D. A., Berger, V. I., & Moring, B. C. (2005). Porphyry copper deposits of the world: database, map, grade and tonnage models. U.S. Geological Survey Open-File Report 2005–1060, http://pubs.usgs.gov/of/2005/1060/.

Singer, D. A., Berger, V. I., & Moring, B. C. (2008). Porphyry copper deposits of the world—database and grade and tonnage models, 2008. U.S. Geological Survey Open-File Report 2008–1155, http://pubs.usgs.gov/of/2008/1155/.

Thoman, M. W., Zonge, K. L., & Liu, D. (2000). Geophysical case history of North Silver Bell, Pima County, Arizona—a supergene-enriched porphyry copper deposit. In R. B. Ellis, R. Irvine, & F. Fritz (Eds.), Northwest Mining Association 1998 Practical Geophysics Short Course Selected Papers on CD-ROM: Spokane. Washington: Northwest Mining Association.

Tzeng, G. H., & Huang, J. J. (2011). *Multiple attribute decision making: Methods and applications*. New York: CRC Press.

Verduzco, B., Fairhead, J. D., Green, C. M., & MacKenzie, C. (2004). New insights into magnetic derivatives for structural mapping. *The Leading Edge, 23*, 116–119.

Yoon, K., & Hwang, C. L. (1995). *Multiple attribute decision making: An introduction*. Thousand Oaks: Sage.

Yousefi, M., & Carranza, E. J. M. (2015). Data-driven index overlay and Boolean logic mineral prospectivity modeling in greenfields exploration. *Natural Resources Research*. doi:10.1007/s11053-014-9261-9.

Zeleny, M. (1982). *Multiple criteria decision making*. New York: McGraw-Hill.

Zuo, R., & Carranza, E. J. M. (2011). Support vector machine: A tool for mapping mineral prospectivity. *Computers & Geosciences, 37*, 1967–1975.